chemistry

MDPI

Article

Self-Assembly and Gelation Study of Dipeptide Isomers with Norvaline and Phenylalanine

Erica Scarel [1], Giovanni Pierri [2], Petr Rozhin [1], Simone Adorinni [1], Maurizio Polentarutti [3], Consiglia Tedesco [2,*] and Silvia Marchesan [1,*]

[1] Chemical and Pharmaceutical Sciences Department, University of Trieste, 34127 Trieste, TRS, Italy
[2] Department of Chemistry and Biology "A. Zambelli", University of Salerno, 84084 Fisciano, SA, Italy
[3] Elettra-Sincrotrone Trieste, S.S. 114 km 163.5, Basovizza (TS), 34149 Trieste, TRS, Italy
* Correspondence: ctedesco@unisa.it (C.T.); smarchesan@units.it (S.M.)

Abstract: Dipeptides have emerged as attractive building blocks for supramolecular materials thanks to their low-cost, inherent biocompatibility, ease of preparation, and environmental friendliness as they do not persist in the environment. In particular, hydrophobic amino acids are ideal candidates for self-assembly in polar and green solvents, as a certain level of hydrophobicity is required to favor their aggregation and reduce the peptide solubility. In this work, we analyzed the ability to self-assemble and the gel of dipeptides based on the amino acids norvaline (Nva) and phenylalanine (Phe), studying all their combinations and not yielding to enantiomers, which display the same physicochemical properties, and hence the same self-assembly behavior in achiral environments as those studied herein. A single-crystal X-ray diffraction of all the compounds revealed fine details over their molecular packing and non-covalent interactions.

Keywords: self-assembly; gels; crystals; XRD; supramolecular chemistry; norvaline; phenylalanine; chirality; D-amino acids; peptides

Citation: Scarel, E.; Pierri, G.; Rozhin, P.; Adorinni, S.; Polentarutti, M.; Tedesco, C.; Marchesan, S. Self-Assembly and Gelation Study of Dipeptide Isomers with Norvaline and Phenylalanine. *Chemistry* **2022**, *4*, 1417–1428. https://doi.org/10.3390/chemistry4040093

Received: 10 October 2022
Accepted: 31 October 2022
Published: 2 November 2022

1. Introduction

Dipeptides have attracted researchers' interests as building blocks for supramolecular materials thanks to their chemical diversity, low cost and ease of preparation, inherent biocompatibility, and biodegradability so that they do not persist in the environment as pollutants [1–5]. In this area, diphenylalanine clearly plays a pivotal role [6–10], and simple chemical variations have proved effective in tailoring its assembly into a variety of elongated nanostructures [11–16], nanoparticles [17–19] or attaining control over the nanotubes' diameter and their hydrogelation [20]. Nevertheless, diphenylalanine is mostly known for its strong propensity to assemble into microtubes that arise from the hierarchical bundling of nanotubes [6], whose inner cavity is water-filled and defined by six dipeptide molecules arranged head—to—tail, as revealed by its crystal structure [21,22].

Conversely, the substitution of one phenylalanine with another hydrophobic amino acid sometimes hinders the dipeptide's ability to self-assemble into supramolecular water-filled channels in ways that are difficult to predict [23]. For example, Ile-Phe [24] and Phe-Ile [25] crystal structures display an alternation of hydrophobic and hydrophilic layers, yet the former was reported to yield nanofibrillar hydrogels [26]. Interestingly, the stereoisomer D-Phe-L-Ile, but not D-Ile-L-Phe, could instead assemble into water-filled channels that formed supramolecular hydrogels [27]. In the case of the homolog peptides with Val (sidechain = -$CH(CH_3)_2$) in place of Ile (sidechain = -$CH(CH_3)CH_2CH_3$), neither homochiral Val-Phe nor Phe-Val could self-assemble under the tested conditions [26,28], and their crystal structures revealed a supramolecular packing into amphipathic layers [29,30]. Interestingly, also, in this case, a simple change in the amino acid chirality from L- to D- was sufficient to restore the nanotube formation ability for D-Phe-L-Val, but not for D-Val-L-Phe [31].

Valine is a naturally occurring amino acid with a propyl sidechain that is branched at the β-carbon, just as Ile and its linear analog norvaline (Nva) is not found in today's proteomes; although it may have been an abundant protein component during the early stages of biological evolution [32]. This hypothesis raises interesting questions as to the relevance of the branched sidechain on the amino acid's ability to pack into defined supramolecular structures. Furthermore, Nva is attracting researchers' interests in new uses in therapy. For instance, Nva has been known to reduce blood pressure and promote diuresis, in the hypertension of rat models [33,34]. As a first step to shedding light on this exciting area pertaining to Nva structural studies, we thus prepared the analogous series of homochiral (i.e., with both L-amino acids) and heterochiral (i.e., with D-Phe and L-Nva) Nva-Phe and Phe-Nva dipeptides and studied their crystal packing and ability to gel.

2. Materials and Methods

2.1. Materials and General Methods

Fmoc-amino acids, 2-chlorotrityl chloride resin, and coupling agents were obtained from GL Biochem (Shanghai, China) Ltd. All other chemicals and solvents were acquired at an analytical grade from Merck. An in-line Millipore RiOs/Origin system provided high-purity Milli-Q-water with a resistivity >18 M Ω cm. ^{1}H-NMR and ^{13}C-NMR spectra were recorded using a Varian Innova spectrometer at 400 MHz, with chemical shifts reported as ppm (using tetramethylsilane as the internal standard). LC-MS analyses were performed on an Agilent 6120 (Milan, Italy) coupled with an electrospray-ionization mass spectrometer (ESI-MS, quadrupole detector). Optical microscopy images were acquired on a drop of the fresh samples deposited on clean glass slides, and pictures were taken with the microscope software ZEISS 3.3.

2.2. Dipeptide Synthesis and Purification

All peptides were synthetized in a solid phase with a Fmoc-protection strategy [31]. The crude was purified with HPLC Agilent 6120 as an instrument and the C-18 column (Kinetex, 5 μm, 100 Å, 250 × 10 mm, Phenomenex). All samples were dissolved in an H_2O/MeCN 75/25 mixture. Acetonitrile (MeCN) and water with 0.05% trifluoroacetic acid (TFA) as a mobile phase were eluted with the following method: t = 0 min. 15% MeCN; t = 2 min 15% MeCN; t = 13 min. 45% MeCN; t = 15 min. 95% MeCN; t = 17 min. 95% MeCN.

2.3. Circular Dichroism

Peptides were dissolved in milli-Q-water at 5 mM, and the pH was corrected with NaOH 1 M to reach the final value of 7.0. Samples were then placed in a 0.1 mm quartz cuvette on a Jasco J-815 spectropolarimeter at 25 °C (Peltier), with a 1 nm resolution and a speed of 50 nm/min. The plotted spectra were obtained as an average of the 25 accumulations in order to increase the signal/noise ratio.

2.4. Self-Assembly Tests

All peptides were tested in different solvents, as described in Section 3.2. Hydrogelation tests were also performed in a phosphate-buffered saline (PBS) buffer (phosphate buffer 0.1 M pH = 7.0, NaCl 1.37 M, KCl 27 mM). In all cases, 1 mg of the compounds 1–4 were added to 0.1 mL of solvent (final concentration 38 mM) and gently swirled at room temperature. If the compound was soluble, then its concentration was increased until saturation.

2.5. Transmission Electron Microscopy (TEM)

A sample was prepared by dissolving compound **4** in MeCN at its minimum gelling concentration (mgc). The fresh gel was transferred onto TEM carbon grids previously exposed to a UV-Ozone Procleaner Plus for 5 min. A drop of aqueous tungstate phosphate solution (pH 7.2) was added as the contrast agent, and all the samples were dried in vacuo. The images were recorded on a Philips EM 208 microscope operating at 100 kV and equipped with an 11 MP bottom-mounted CCD Olympus Quemesa camera.

2.6. Raman Microspectroscopy

All peptides were crystallized in a PBS buffer with D-Phe-L-Nva also in MeCN, and some crystals were placed on a glass slide and left to dry in vacuo. Raman spectra were acquired using a 532 nm laser at 500 mW (5–10% power) with a Renishaw instrument. Spectra were recorded with 10 accumulations in several spots per sample, with a 1 cm^{-1} resolution.

2.7. Single-Crystal X-ray Diffraction (XRD)

Single crystals of all the compounds in PBS were collected with a loop before being cryoprotected by dipping them in glycerol, and they were then stored frozen in liquid nitrogen. The crystals were mounted on the diffractometer at the Synchrotron Elettra (Trieste, Italy), beamline XRD2, using the robot available at the facility. The temperature was kept at 100 K by a stream of nitrogen on the crystals. Diffraction data were collected by rotating the crystal using a synchrotron radiation wavelength of 0.6200 Å, with a rotation interval of 0.5°/image and a crystal-to-detector distance of 150 mm. Further details can be found in the Supplementary Materials.

3. Results and Discussion

3.1. Dipeptide Preparation and Spectroscopic Characterization

The four dipeptides shown in Figure 1 were prepared and studied in this work, and they represent all possible combinations of Nva and Phe in the linear dipeptides that were not enantiomers since their mirror-images display the same physicochemical properties and self-assembly behavior in achiral environments. Compounds **1–4** were prepared by solid-phase synthesis based on Fmoc N-protection [31] and were purified by a reversed-phase HPLC. Their identity and purity were confirmed by ^{1}H-NMR, ^{13}C-NMR, and ESI-MS (see Supplementary Materials and Figures S1–S20). Their HPLC retention times (Rt), which can be considered an experimental measure of hydrophobicity [35], were in the order of **1** < **3** < **2** ~**4**, confirming the two heterochiral dipeptides **2** and **4** as the most hydrophobic isomers of the series (see Supplementary Materials, Figure S21 and Table S1).

The increased hydrophobicity of the heterochiral **2** and **4** relative to the homochiral **1** and **3** may be ascribed to differences in the dipeptides' preferred conformations. To verify this hypothesis, the four compounds were analyzed in an aqueous solution at a neutral pH by circular dichroism (CD). The CD spectra (Supplementary Materials, Figure S22) were reminiscent of those displayed by the dipeptide analogs with Val in place of Nva [31]. In particular, their spectral signature was characterized by two peaks at 198 and 218 nm that can be representative of a population of conformations whose majority have dihedral angles that are typical for β-structures [36]. Furthermore, if we also consider that the enantiomers will display a mirror-image CD spectra that is reflected on the x axis, then we can conclude that the CD signal above 200 nm is dictated by the chirality of Phe (i.e., a positive for L-Phe and negative for D-Phe) [37], irrespective of its position along the sequence. Overall, the CD spectra did not show dramatic differences between the Nva and the Val series.

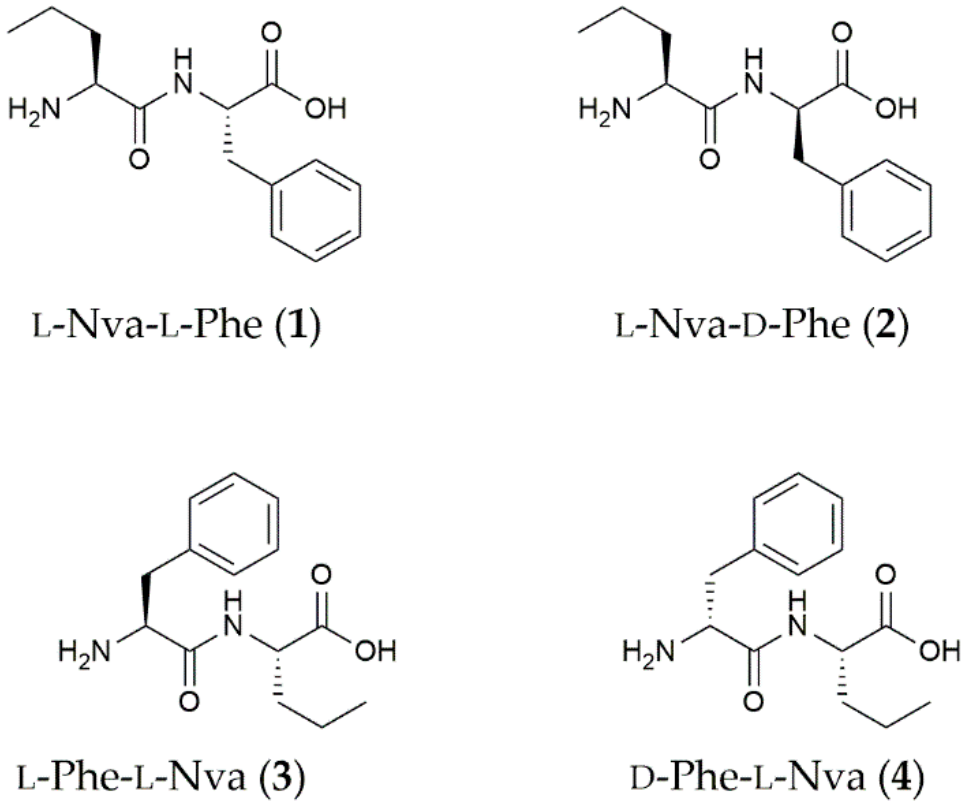

Figure 1. The four dipeptides of this study represent all combinations of Nva and Phe in linear dipeptides that are not enantiomeric couples, which display the same physico-chemical properties (i.e., D-Nva-D-Phe, D-Nva-L-Phe, D-Phe-D-Nva, and L-Phe-D-Nva are the enantiomers of compounds **1–4**, respectively, and they were thus not synthesized).

3.2. Self-Assembly Tests

The self-assembly of the four dipeptides was probed in a saline phosphate buffer (PBS) and a variety of green solvents, as shown in Table 1. Remarkably, in the vast majority of the tested conditions, all four compounds crystallized. At high concentrations (>100 mM), heterochiral **4** initially formed short fibrils that rapidly interconverted into crystals (see Supplementary Materials, Figure S23). Compound **4** was also the only one to gel in acetonitrile but then rapidly converted into crystals (see Figure 2), thus not allowing for the rheological characterization of the gel viscoelastic properties. The gel was also analyzed by transmission electron microscopy (TEM) as quickly as possible, but only crystals were seen (Supplementary Materials, Figure S24).

Table 1. Self-assembly tests in various solvents for compounds **1–4**.

Solvent	L-Nva-L-Phe (1)	L-Nva-D-Phe (2)	L-Phe-L-Nva (3)	D-Phe-L-Nva (4)
PBS buffer	Crystal	Crystal	Crystal	Crystal
MeOH	Crystal	Crystal	Crystal	Crystal
EtOH	Crystal	Crystal	Crystal	Crystal
*i*PrOH	Crystal	Crystal	Crystal	Crystal
MeCN	Crystal	Crystal	Crystal	Gel [1]
Acetone	Precipitate	Precipitate	Precipitate	Precipitate
Argan oil	Precipitate	Precipitate	Precipitate	Precipitate

[1] Metastable gel that rapidly converts into crystals.

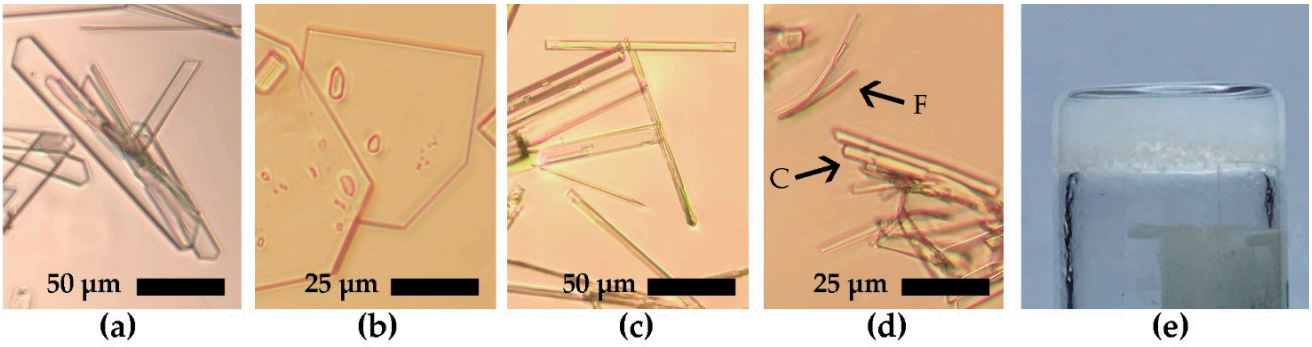

Figure 2. Optical microscope photographs of dipeptide crystals in PBS: (**a**) **1**, (**b**) **2**, (**c**) **3**, and (**d**) **4** (F indicates fibrils and C crystals). (**e**) Photograph of **4** metastable gel in MeCN.

3.3. Raman Spectroscopy

Raman spectroscopy has recently been applied to peptide assemblies [38–42] and was also employed here to compare the signals of each dipeptide in their powder and crystal forms (Figure 3). All the spectra were dominated by the Phe signals at 1003 cm^{-1} and 1034 cm^{-1}. Both these modes can be assigned to sidechain vibrational motions of the aromatic ring. In particular, the former signal can be ascribed to the benzene breathing mode, while the latter band was due to the in-plane CH bending [43,44]. New signals (denoted with * in Figure 3) arose with self-assembly in all cases, of which those at 1240–1260 cm^{-1} and 1657–1687 cm^{-1} were assigned to the amide III and I bands, respectively, as extended H-bond networks formed in the β-sheet-like stacks [42]. The Raman spectra of compound **4** crystals in MeCN displayed analogous peptide signals in PBS, suggesting the same supramolecular packing (see Supplementary Materials, Figure S25).

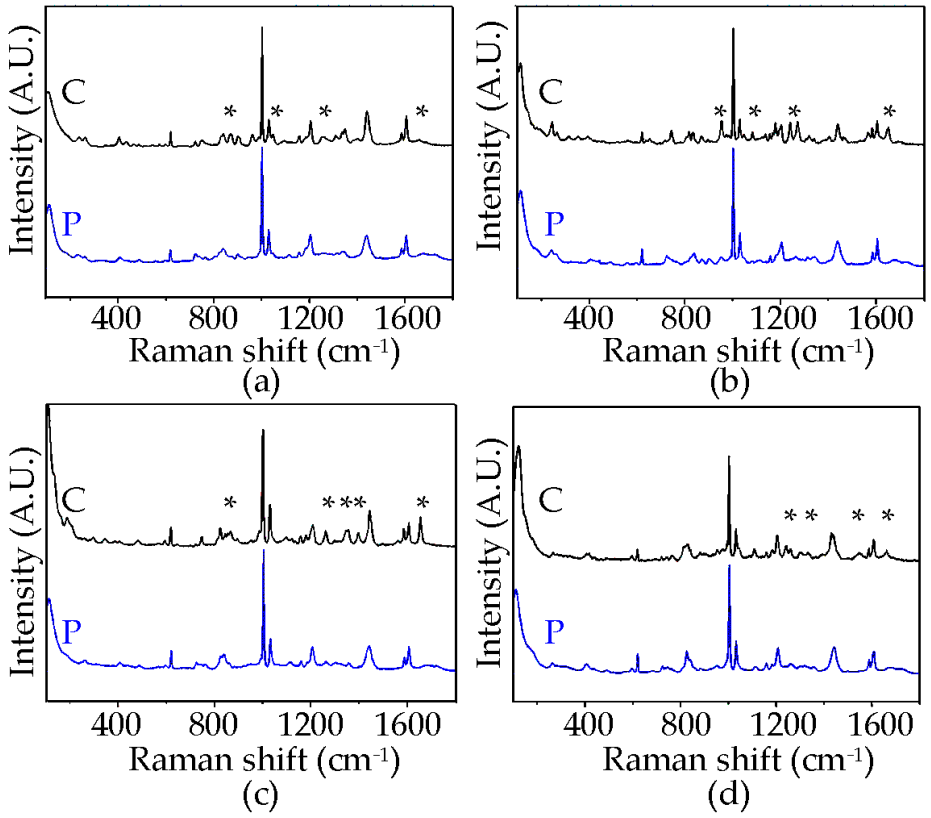

Figure 3. Raman spectra of the four compounds in the crystal (C, black traces) and powder (P, blue traces) in forms: (**a**) **1**; (**b**) **2**; (**c**) **3**; (**d**) **4**. * denotes signals arising in the crystal forms.

3.4. Single-Crystal X-ray Diffraction

The solid-state assembly of the two dipeptide stereoisomers **1** and **2** are very similar. In particular, **1** crystallizes as a hydrate crystal form (host: guest ratio of 1:2) in an orthorhombic system (space group $P2_12_12_1$). Interestingly, no channels can be highlighted; instead, water molecules are localized in small pockets and appear to be fundamental for the crystal packing (Figure 4). The typical $–NH_3^+\cdots{}^-OOC–$ groups and H-bond pattern [20] are missing, and all three H atoms of the terminal amine group interacted with the guest molecules. Host–host interactions involving the carbonyl oxygen atom O3 and the hydrogen atom of the amide group (N2···O3 = 2.825(1) Å, N2-H2···O3 = 2.02 Å, N2-H2···O3 = 151.0°) and the carbonyl oxygen atom O1 and hydrogen atom were attached to the α carbon C1 (C1···O1 = 3.343(1) Å, C1-H1···O1 = 2.59 Å, N2-H2···O3 = 131.7°). This H-bond pattern ensured the alignment of the dipeptides along the shortest *a* axis.

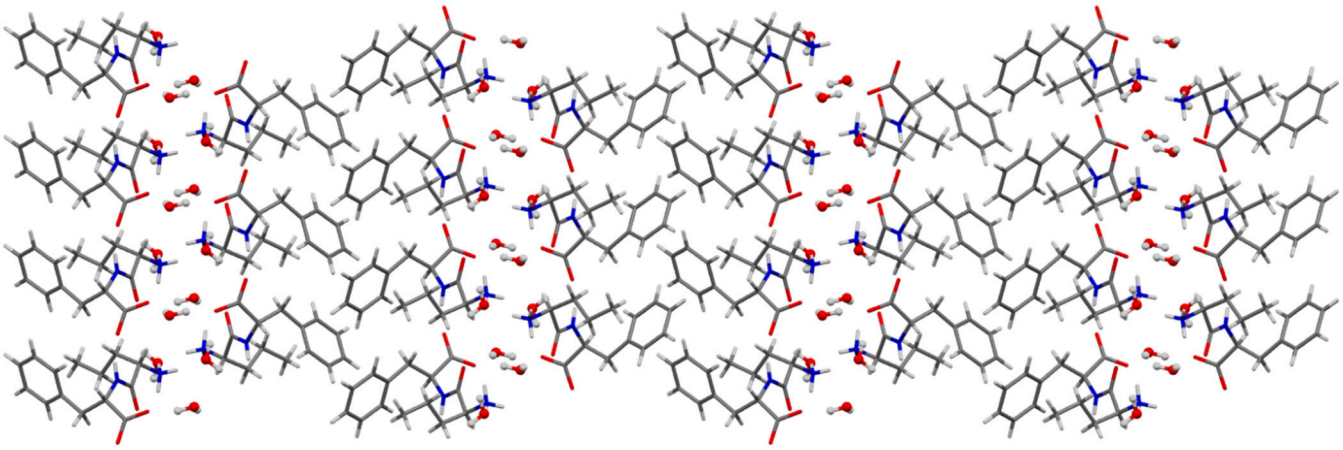

Figure 4. Dipeptide **1** crystal packing as viewed along the *b* axis (CCDC 2210050).

Dipeptide **2** crystallizes as a hydrate crystal form (with a host:guest ratio of 1:2) in a monoclinic system (space group $P2_1$). As for dipeptide **1**, its stereoisomer **2** does not form water channels, and the water molecules are localized in pockets between the dipeptides (Figure 5). The analysis of the H-bond pattern involving the $–NH_3^+\cdots{}^-OOC–$ groups revealed a significant difference between the two crystal structures. In particular, two amino H atoms formed H-bonds with two water molecules in the crystal structure, while the third one interacted with the carbonyl oxygen atom O2 (N1···O2 = 2.844(1) Å, N1-H1A···O2 = 1.96 Å, N1-H1A···O2 = 165.0°). As reported for the crystal structure of dipeptide **1**, an NH···OC hydrogen bond (N2···O3 = 2.968(1) Å, N2-H2···O3 = 2.10 Å, N2-H2···O3 = 167.2°) ensured the dipeptides alignment along the shortest *a* axis.

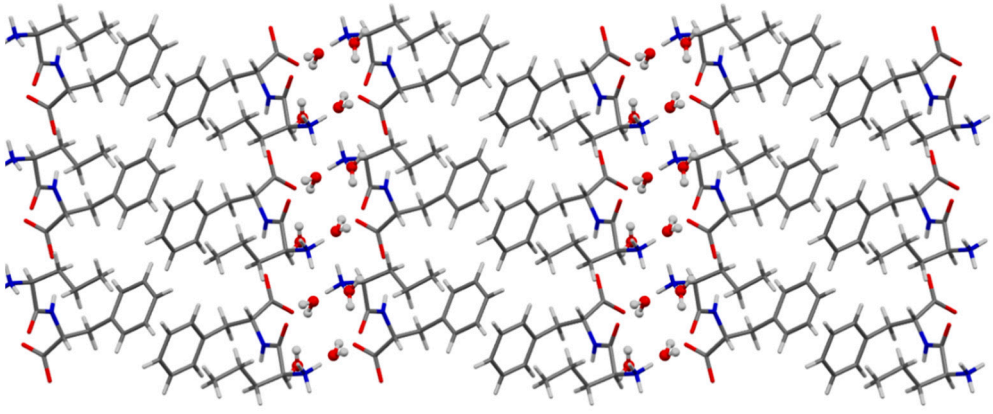

Figure 5. Dipeptide **2** crystal packing as viewed along the *b* axis (CCDC 2210051).

The H-bond arrangement between the host and guest molecules in the two solid-state assemblies is very similar, with one minor exception. In both cases, the two water molecules helped to bridge the dipeptides aligned along the *a* axis; however, in the crystal structure of homochiral **1**, the water molecule O2W (depicted in green in Figure 6a) formed the third H-bond with another dipeptide aligned along the *c* axis (Figure S27 in the ESI). Furthermore, both **1** and **2** display a layered packing structure with hydrophobic regions defined by the hydrophobic CH–π interactions [45,46] between the sidechains and hydrophilic regions where the water molecules are confined.

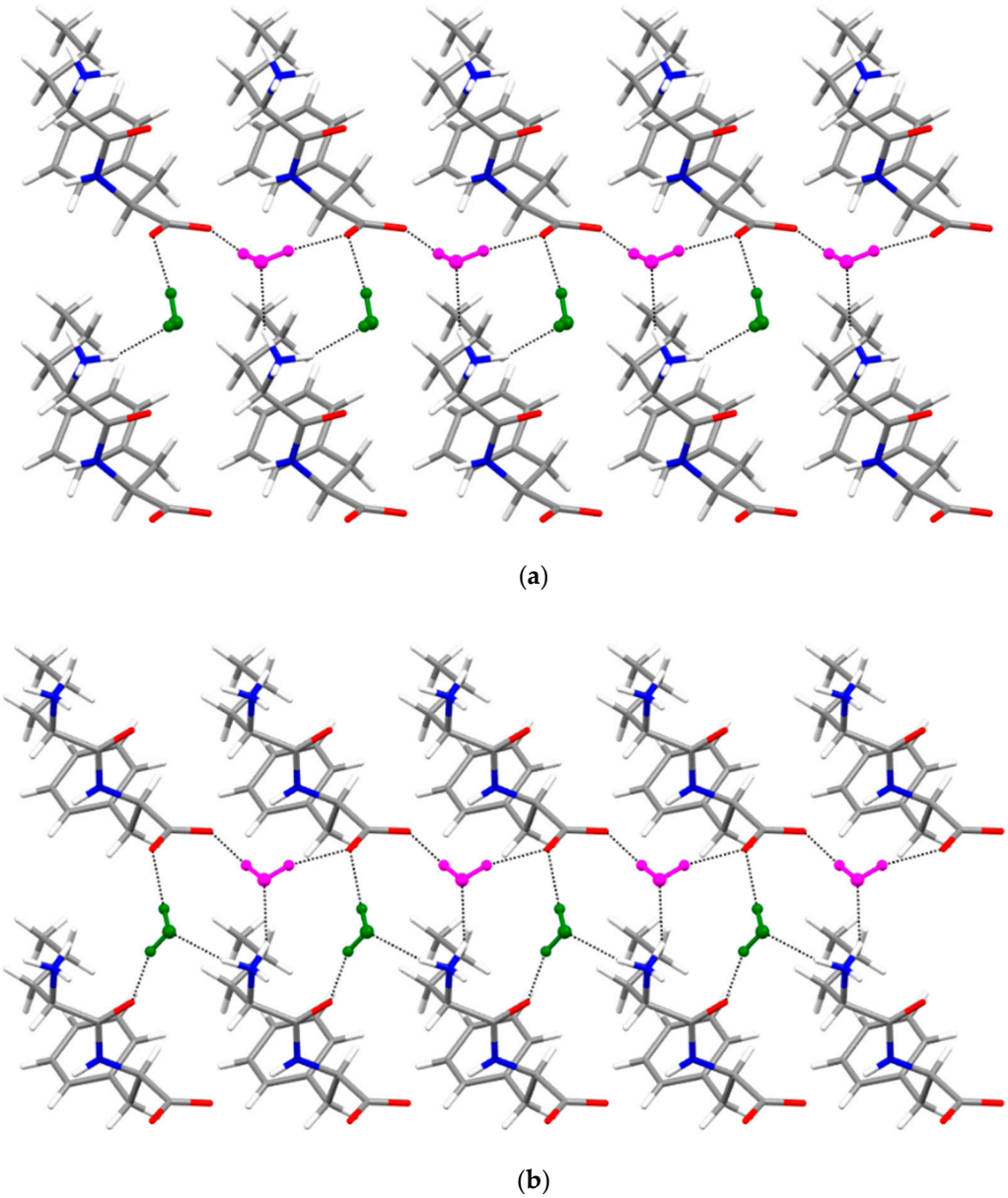

Figure 6. Host–guest H-bond pattern in (**a**) homochiral **1** and (**b**) heterochiral **2**. Water molecule O1W is depicted in magenta, O2W in green. Host–host interactions were removed for clarity.

Conversely, the crystal structures of the dipeptide stereoisomers **3** and **4** are quite different from each other, although both form water layers parallel to the shortest unit cell axis. In particular, **3** crystallized as a hydrate crystal form in an orthorhombic system (space group $P2_12_12_1$) with the amide-rich region filled with water molecules and the sidechains segregated into the hydrophobic region, establishing weak hydrophobic interactions (Figure 7). Because of the highly disordered water molecules, a solvent mask

procedure was applied. In particular, 118 electrons were found in a volume of 252 Å^3 which was consistent with the presence of three water molecules per asymmetric unit.

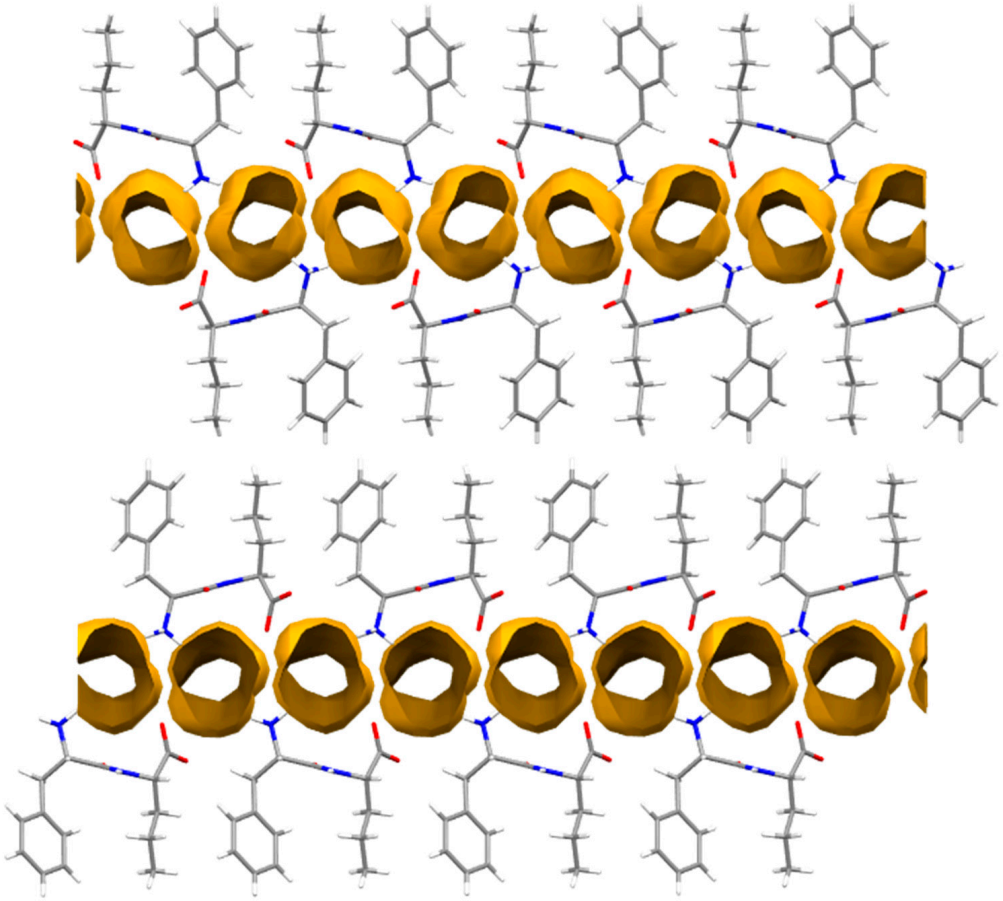

Figure 7. Crystal packing of **3** (CCDC 2210055) as viewed along the *a* axis with the water layer depicted in gold.

No H-bonds can be highlighted between the –NH_3^+ and $^-$OOC– groups. Using a preliminary model with highly disordered water molecules, it was possible to point out that all three of the amino H atoms of the –NH_3^+ group established weak interactions with the guest molecules. Furthermore, the dipeptides were aligned along the shortest *a* axis mainly through H-bonds involving the carbonyl oxygen atoms O1 (N2···O1 = 2.837(1) Å, N2H2···O1 = 1.97 Å, N2H2···O1 = 168.3°) and O3 (C3···O3 = 3.305(2) Å, C3H3···O3 = 2.37 Å, N2H2···O1 = 154.6°).

Finally, dipeptide **4** crystallized as a hydrate crystal form (with a host: guest ratio of 1:2) in a monoclinic system (space group *C*2) (Figure 8). The crystal structure revealed layers parallel to the shortest *b*-axis filled with water molecules showing full occupancy. The crystal structure exhibited the typical H-bond pattern of the Phe–Phe class described by Görbitz [23], with two amino H atoms interacting with two carboxylic oxygen atoms of two distinct dipeptides, while the third one interacted with the water molecule O1W inside the water layer. Other host–guest interactions involved the $^-$OOC– group and water molecule O2W, which bridged together the two dipeptides along the *c* axis. Notably, the water molecules established a beautiful guest–guest H-bond network, which appeared to be fundamental for the solid-state assembly (Figure 9).

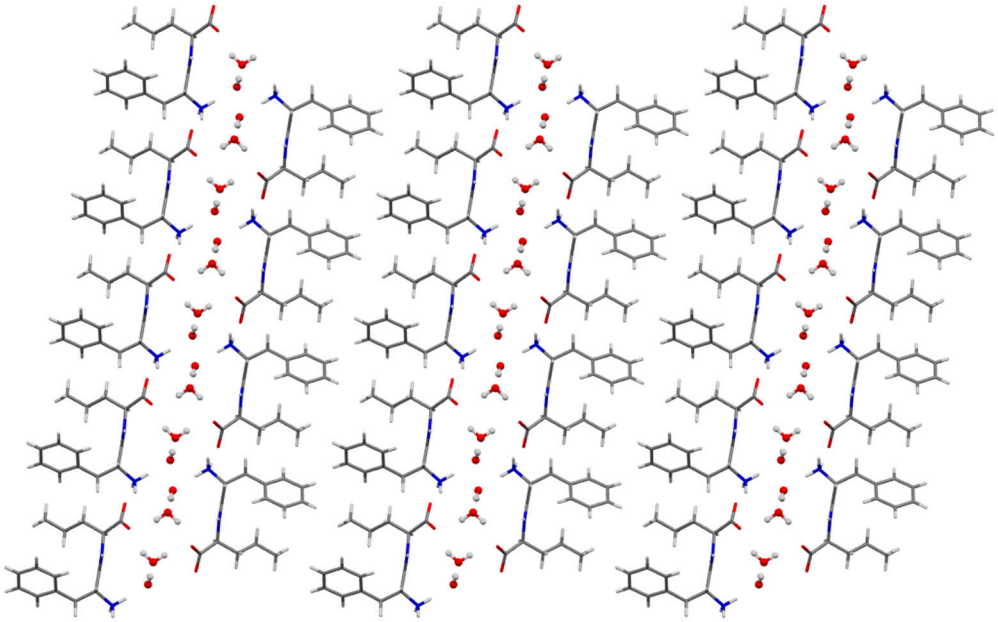

Figure 8. Dipeptide **4** crystal packing as viewed along the *b* axis (CCDC 2210056).

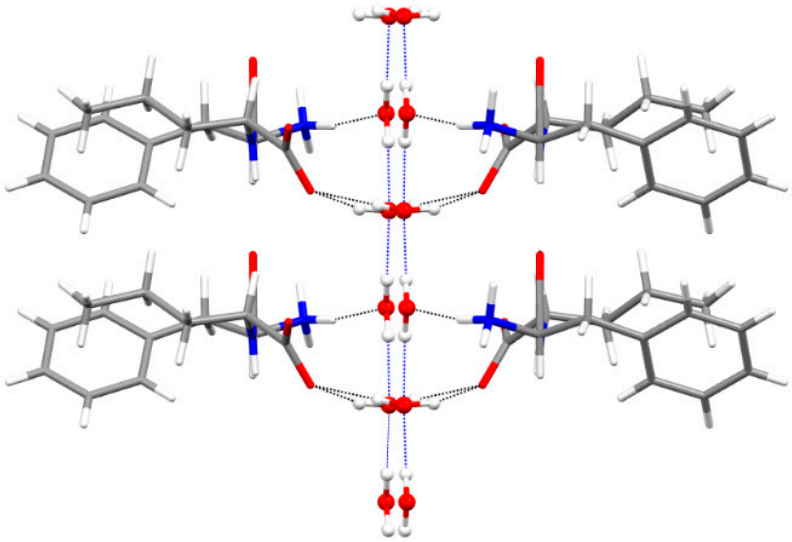

Figure 9. Host–guest and guest–guest H-bonds in dipeptide **4** depicted in dotted black and blue lines, respectively.

4. Conclusions

In conclusion, the substitution of one Phe in diphenylalanine with the Nva amino acid completely hinders the ability of the dipeptide to self-assemble into water-filled channels and gelling nanotubes. Heterochirality is associated with an increase in the hydrophobicity of the dipeptides, and only heterochiral compound **4** was able to form metastable gels in the acetonitrile that rapidly converted into crystals. Indeed, all the tested compounds displayed a marked tendency towards crystallization in polar solvents, and overall, the supramolecular behavior was very similar to the analogs with Val in place of Nva. One marked difference, however, is that the Val analog, when compared to compound **4,** displayed the ability to form water-filled nanotubes that yielded hydrogels in the PBS [31]. It is possible that the linear sidechain of Nva has simply more conformational freedom to enable tight packing into crystals with a layered structure relative to the branched sidechain of Val.

Further studies are ongoing in our laboratories with the linear homolog norleucine, which is the structural isomer of branched leucine, in an attempt to identify more general trends in the self-assembly behavior of hydrophobic dipeptides. In the future, advancing knowledge on the ability of simple dipeptides to form supramolecular hydrophilic channels may assist their design for insertion into biological membranes, for instance, towards therapeutic effects [47–49]. Further scope for applications of Nva-bearing dipeptides may also arise as current studies are revealing new beneficial effects from the administration of this amino acid in diverse pathological settings, spanning from neurodegeneration to hypertension [50–54].

Supplementary Materials: The following supporting information can be downloaded at: https://www.mdpi.com/article/10.3390/chemistry4040093/s1, 1H-NMR, 13C-NMR, and ESI-MS spectroscopic characterization of the four dipeptides (Figures S1–S20), HPLC traces and retention times (Figure S21 and Table S1), CD spectra (Figure S22), optical microscopy images (Figure S23), TEM imaging (Figure S24), Raman spectra (Figure S25), XRD data (Figures S26 and S27 and Table S2). References [55–60] are cited in the Supplementary Materials file.

Author Contributions: Investigation, E.S., G.P., P.R. and S.A.; data curation, E.S., G.P., P.R. and M.P.; supervision, M.P., C.T. and S.M.; conceptualization, S.M.; methodology, M.P., C.T. and S.M.; writing—original draft preparation, E.S., G.P. and S.M.; writing—review and editing, E.S., G.P., P.R., S.A., M.P., C.T. and S.M. All authors have read and agreed to the published version of the manuscript.

Funding: This research received funding from the University of Trieste (FRA2022 to S.M.).

Institutional Review Board Statement: Not applicable.

Informed Consent Statement: Not applicable.

Data Availability Statement: Data are available in the Supporting Materials file and from the authors upon reasonable request.

Acknowledgments: We acknowledge Francesca Prochilo at the University of Trieste for administrative assistance. We also acknowledge Elettra Sincrotrone at the University of Trieste for providing access to its synchrotron radiation beamline XRD2.

Conflicts of Interest: The authors declare no conflict of interest.

References

1. Adams, D.J. Dipeptide and tripeptide conjugates as low-molecular-weight hydrogelators. *Macromol. Biosci.* **2011**, *11*, 160–173. [CrossRef] [PubMed]
2. Chen, Y.; Tao, K.; Ji, W.; Makam, P.; Rencus-Lazar, S.; Gazit, E. Self-assembly of cyclic dipeptides: Platforms for functional materials. *Prot. Pept. Lett.* **2020**, *27*, 688–697. [CrossRef] [PubMed]
3. Rissanou, A.N.; Simatos, G.; Siachouli, P.; Harmandaris, V.; Mitraki, A. Self-assembly of alanine-isoleucine and isoleucine-isoleucine dipeptides through atomistic simulations and experiments. *J. Phys. Chem. B* **2020**, *124*, 7102–7114. [CrossRef] [PubMed]
4. Balachandra, C.; Padhi, D.; Govindaraju, T. Cyclic dipeptide: A privileged molecular scaffold to derive structural diversity and functional utility. *ChemMedChem* **2021**, *16*, 2558–2587. [CrossRef] [PubMed]
5. Scarel, M.; Marchesan, S. Diketopiperazine gels: New horizons from the self-assembly of cyclic dipeptides. *Molecules* **2021**, *26*, 3376. [CrossRef]
6. Reches, M.; Gazit, E. Casting metal nanowires within discrete self-assembled peptide nanotubes. *Science* **2003**, *300*, 625–627. [CrossRef]
7. Brahmachari, S.; Arnon, Z.A.; Frydman-Marom, A.; Gazit, E.; Adler-Abramovich, L. Diphenylalanine as a reductionist model for the mechanistic characterization of β-amyloid modulators. *ACS Nano* **2017**, *11*, 5960–5969. [CrossRef]
8. Safaryan, S.; Slabov, V.; Kopyl, S.; Romanyuk, K.; Bdikin, I.; Vasilev, S.; Zelenovskiy, P.; Shur, V.Y.; Uslamin, E.A.; Pidko, E.A.; et al. Diphenylalanine-based microribbons for piezoelectric applications via inkjet printing. *ACS Appl. Mater. Interfaces* **2018**, *10*, 10543–10551. [CrossRef]
9. Zelenovskiy, P.S.; Domingues, E.M.; Slabov, V.; Kopyl, S.; Ugolkov, V.L.; Figueiredo, F.M.L.; Kholkin, A.L. Efficient water self-diffusion in diphenylalanine peptide nanotubes. *ACS Appl. Mater. Interfaces* **2020**, *12*, 27485–27492. [CrossRef]
10. Erdoğan, H. Cation-based approach to morphological diversity of diphenylalanine dipeptide structures. *Soft Matter* **2021**, *17*, 5221–5230. [CrossRef]

11. Diaferia, C.; Roviello, V.; Morelli, G.; Accardo, A. Self-assembly of pegylated diphenylalanines into photoluminescent fibrillary aggregates. *Chemphyschem* **2019**, *20*, 2774–2782. [CrossRef] [PubMed]
12. Rajbhandary, A.; Nilsson, B.L. Investigating the effects of peptoid substitutions in self-assembly of fmoc-diphenylalanine derivatives. *Biopolymers* **2017**, *108*, e22994. [CrossRef] [PubMed]
13. Martin, A.D.; Wojciechowski, J.P.; Robinson, A.B.; Heu, C.; Garvey, C.J.; Ratcliffe, J.; Waddington, L.J.; Gardiner, J.; Thordarson, P. Controlling self-assembly of diphenylalanine peptides at high ph using heterocyclic capping groups. *Sci. Rep.* **2017**, *7*, 43947. [CrossRef] [PubMed]
14. Karikis, K.; Butkiewicz, A.; Folias, F.; Charalambidis, G.; Kokotidou, C.; Charisiadis, A.; Nikolaou, V.; Nikoloudakis, E.; Frelek, J.; Mitraki, A.; et al. Self-assembly of (boron-dipyrromethane)-diphenylalanine conjugates forming chiral supramolecular materials. *Nanoscale* **2018**, *10*, 1735–1741. [CrossRef] [PubMed]
15. Dudukovic, N.A.; Hudson, B.C.; Paravastu, A.K.; Zukoski, C.F. Self-assembly pathways and polymorphism in peptide-based nanostructures. *Nanoscale* **2018**, *10*, 1508–1516. [CrossRef]
16. Diaferia, C.; Avitabile, C.; Leone, M.; Gallo, E.; Saviano, M.; Accardo, A.; Romanelli, A. Diphenylalanine motif drives self-assembling in hybrid pna-peptide conjugates. *Chem. Eur. J.* **2021**, *27*, 14307–14316. [CrossRef]
17. Garcia, A.M.; Melchionna, M.; Bellotto, O.; Kralj, S.; Semeraro, S.; Parisi, E.; Iglesias, D.; D'Andrea, P.; De Zorzi, R.; Vargiu, A.V.; et al. Nanoscale assembly of functional peptides with divergent programming elements. *ACS Nano* **2021**, *15*, 3015–3025. [CrossRef]
18. Li, S.; Liu, Y.; Xing, R.; Yan, X. Covalently assembled dipeptide nanoparticles with adjustable fluorescence emission for multicolor bioimaging. *ChemBioChem* **2019**, *20*, 555–560. [CrossRef]
19. Yuran, S.; Razvag, Y.; Das, P.; Reches, M. Self-assembly of azide containing dipeptides. *J. Pept. Sci.* **2014**, *20*, 479–486. [CrossRef]
20. Kralj, S.; Bellotto, O.; Parisi, E.; Garcia, A.M.; Iglesias, D.; Semeraro, S.; Deganutti, C.; D'Andrea, P.; Vargiu, A.V.; Geremia, S.; et al. Heterochirality and halogenation control phe-phe hierarchical assembly. *ACS Nano* **2020**, *14*, 16951–16961. [CrossRef]
21. Görbitz, C.H. Nanotube formation by hydrophobic dipeptides. *Chem. Eur. J.* **2001**, *7*, 5153–5159. [CrossRef]
22. Görbitz, C.H. The structure of nanotubes formed by diphenylalanine, the core recognition motif of alzheimer's beta-amyloid polypeptide. *Chem. Commun.* **2006**, 2332–2334. [CrossRef] [PubMed]
23. Görbitz, C.H. Microporous organic materials from hydrophobic dipeptides. *Chem. Eur. J.* **2007**, *13*, 1022–1031. [CrossRef] [PubMed]
24. Görbitz, C. L-isoleucyl-L-phenylalanine dihydrate. *Acta Cryst. C* **2004**, *60*, o371–o373. [CrossRef]
25. Görbitz, C. L-phenylalanyl- L-isoleucine 0.88-hydrate. *Acta Cryst. C* **2004**, *60*, o810–o812. [CrossRef]
26. de Groot, N.S.; Parella, T.; Aviles, F.X.; Vendrell, J.; Ventura, S. Ile-phe dipeptide self-assembly: Clues to amyloid formation. *Biophys. J.* **2007**, *92*, 1732–1741. [CrossRef]
27. Bellotto, O.; Kralj, S.; Melchionna, M.; Pengo, P.; Kisovec, M.; Podobnik, M.; De Zorzi, R.; Marchesan, S. Self-assembly of unprotected dipeptides into hydrogels: Water-channels make the difference. *ChemBioChem* **2022**, *23*, e202100518. [CrossRef]
28. Kurbasic, M.; Semeraro, S.; Garcia, A.M.; Kralj, S.; Parisi, E.; Deganutti, C.; De Zorzi, R.; Marchesan, S. Microwave-assisted cyclization of unprotected dipeptides in water to 2,5-piperazinediones and self-assembly study of products and reagents. *Synthesis* **2019**, *51*, 2829–2838. [CrossRef]
29. Görbitz, C. β turns, water cage formation and hydrogen bonding in the structures of L-valyl-L-phenylalanine. *Acta Cryst. B* **2002**, *58*, 512–518. [CrossRef]
30. Görbitz, C. An NH_3^+ ... Phenyl interaction in L-phenylalanyl- L-valine. *Acta Cryst. C* **2000**, *56*, 1496–1498. [CrossRef]
31. Bellotto, O.; Pierri, G.; Rozhin, P.; Polentarutti, M.; Kralj, S.; D'Andrea, P.; Tedesco, C.; Marchesan, S. Dipeptide self-assembly into water-channels and gel biomaterial. *Org. Biomol. Chem.* **2022**, *20*, 6211–6218. [CrossRef] [PubMed]
32. Alvarez-Carreño, C.; Becerra, A.; Lazcano, A. Norvaline and norleucine may have been more abundant protein components during early stages of cell evolution. *Orig. Life Evol. Biosph.* **2013**, *43*, 363–375. [CrossRef] [PubMed]
33. Pokrovskiy, M.V.; Korokin, M.V.; Tsepeleva, S.A.; Pokrovskaya, T.G.; Gureev, V.V.; Konovalova, E.A.; Gudyrev, O.S.; Kochkarov, V.I.; Korokina, L.V.; Dudina, E.N.; et al. Arginase inhibitor in the pharmacological correction of endothelial dysfunction. *Int. J. Hypertens.* **2011**, *2011*, 515047. [CrossRef] [PubMed]
34. Konovalova, E.A.; Chernomortseva, E.S. The study of the endothelial protective properties of the L-norvaline combination with mexidol in the simulation of L-NAME-induced NO deficiency. *Res. Result Pharmacol.* **2019**, *5*, 41–46. [CrossRef]
35. Bolt, H.L.; Williams, C.E.J.; Brooks, R.V.; Zuckermann, R.N.; Cobb, S.L.; Bromley, E.H.C. Log D versus HPLC derived hydrophobicity: The development of predictive tools to aid in the rational design of bioactive peptoids. *Pept. Sci.* **2017**, *108*, e23014. [CrossRef] [PubMed]
36. Garcia, A.M.; Iglesias, D.; Parisi, E.; Styan, K.E.; Waddington, L.J.; Deganutti, C.; De Zorzi, R.; Grassi, M.; Melchionna, M.; Vargiu, A.V.; et al. Chirality effects on peptide self-assembly unraveled from molecules to materials. *Chem* **2018**, *4*, 1862–1876. [CrossRef]
37. Amdursky, N.; Stevens, M.M. Circular dichroism of amino acids: Following the structural formation of phenylalanine. *ChemPhysChem* **2015**, *16*, 2768–2774. [CrossRef]
38. Mazzier, D.; Mosconi, D.; Marafon, G.; Reheman, A.; Toniolo, C.; Moretto, A. Light-driven topochemical polymerization under organogel conditions of a symmetrical dipeptide-diacetylene system. *J. Pept. Sci.* **2017**, *23*, 155–161. [CrossRef]
39. Profit, A.A.; Vedad, J.; Desamero, R.Z. Peptide conjugates of benzene carboxylic acids as agonists and antagonists of amylin aggregation. *Bioconjug. Chem.* **2017**, *28*, 666–677. [CrossRef]

40. Ronen, M.; Kalanoor, B.S.; Oren, Z.; Ron, I.; Tischler, Y.R.; Gerber, D. Characterization of peptides self-assembly by low frequency Raman spectroscopy. *RSC Adv.* **2018**, *8*, 16161–16170. [CrossRef]
41. Levine, M.S.; Ghosh, M.; Hesser, M.; Hennessy, N.; DiGuiseppi, D.M.; Adler-Abramovich, L.; Schweitzer-Stenner, R. Formation of peptide-based oligomers in dimethylsulfoxide: Identifying the precursor of fibril formation. *Soft Matter* **2020**, *16*, 7860–7868. [CrossRef] [PubMed]
42. Scarel, E.; Bellotto, O.; Rozhin, P.; Kralj, S.; Tortora, M.; Vargiu, A.V.; De Zorzi, R.; Rossi, B.; Marchesan, S. Single-atom substitution enables supramolecular diversity from dipeptide building blocks. *Soft Matter* **2022**, *18*, 2129–2136. [CrossRef]
43. Hernández, B.; Pflüger, F.; Kruglik, S.G.; Ghomi, M. Characteristic Raman lines of phenylalanine analyzed by a multiconformational approach. *J. Raman Spectrosc.* **2013**, *44*, 827–833. [CrossRef]
44. Fischer, W.B.; Eysel, H.H. Polarized raman spectra and intensities of aromatic amino acids phenylalanine, tyrosine and tryptophan. *Spectrochim. Acta A Mol. Spectrosc.* **1992**, *48*, 725–732. [CrossRef]
45. Thakuria, R.; Nath, N.K.; Saha, B.K. The Nature and Applications of π–π Interactions: A Perspective. *Cryst. Growth Des.* **2019**, *19*, 523–528. [CrossRef]
46. Grabowski, S.J.; Lipkowski, P. Characteristics of X-H···π Interactions: Ab Initio and QTAIM Studies. *J. Phys. Chem. A* **2011**, *115*, 4765–4773. [CrossRef]
47. Picci, G.; Marchesan, S.; Caltagirone, C. Ion channels and transporters as therapeutic agents: From biomolecules to supramolecular medicinal chemistry. *Biomedicines* **2022**, *10*, 885. [CrossRef]
48. Roy, A.; Talukdar, P. Recent advances in bioactive artificial ionophores. *ChemBioChem* **2021**, *22*, 2925–2940. [CrossRef]
49. Wu, X.; Howe, E.N.W.; Gale, P.A. Supramolecular transmembrane anion transport: New assays and insights. *Acc. Chem. Res.* **2018**, *51*, 1870–1879. [CrossRef]
50. Gao, L.; Zhang, J.H.; Chen, X.X.; Ren, H.L.; Feng, X.L.; Wang, J.L.; Xiao, J.H. Combination of L-arginine and L-norvaline protects against pulmonary fibrosis progression induced by bleomycin in mice. *Biomed. Pharmacother.* **2019**, *113*, 108768. [CrossRef]
51. Javrushyan, H.; Nadiryan, E.; Grigoryan, A.; Avtandilyan, N.; Maloyan, A. Antihyperglycemic activity of L-norvaline and L-arginine in high-fat diet and streptozotocin-treated male rats. *Exp. Mol. Pathol.* **2022**, *126*, 104763. [CrossRef] [PubMed]
52. Polis, B.; Gurevich, V.; Assa, M.; Samson, A.O. Norvaline restores the bbb integrity in a mouse model of Alzheimer's disease. *Int. J. Mol. Sci.* **2019**, *20*, 4616. [CrossRef]
53. Polis, B.; Srikanth, K.D.; Gurevich, V.; Gil-Henn, H.; Samson, A.O. L-norvaline, a new therapeutic agent against Alzheimer's disease. *Neural Regen. Res.* **2019**, *14*, 1562–1572. [CrossRef] [PubMed]
54. Gilinsky, M.A.; Polityko, Y.K.; Markel, A.L.; Latysheva, T.V.; Samson, A.O.; Polis, B.; Naumenko, S.E. Norvaline reduces blood pressure and induces diuresis in rats with inherited stress-induced arterial hypertension. *BioMed. Res. Int.* **2020**, *2020*, 4935386. [CrossRef] [PubMed]
55. Battye, T.G.G.; Kontogiannis, L.; Johnson, O.; Powell, H.R.; Leslie, A.G.W. iMOSFLM: A New Graphical Interface for Diffraction-Image Processing with MOSFLM. *Acta Crystallogr. Sect. D* **2011**, *67*, 271–281. [CrossRef] [PubMed]
56. Evans, P.R. Scaling and assessment of data quality. *Acta Crystallogr. Sect. D* **2006**, *62*, 72–82. [CrossRef] [PubMed]
57. Evans, P.R.; Murshudov, G.N. How good are my data and what is the resolution? *Acta Crystallogr. Sect. D Biol. Crystallogr.* **2013**, *69*, 1204–1214. [CrossRef]
58. Sheldrick, G.M. *SHELXT*—Integrated space-group and crystal-structure determination. *Acta Crystallogr. Sect. A* **2015**, *71*, 3–8. [CrossRef]
59. Sheldrick, G.M. Crystal structure refinement with *SHELXT*. *Acta Crystallogr. Sect. C* **2015**, *71*, 3–8. [CrossRef]
60. Dolomanov, O.V.; Bourhis, L.J.; Gildea, R.J.; Howard, J.A.K.; Puschmann, H. OLEX2: A Complete Structure Solution, Refinement and Analysis Program. *J. Appl. Cryst.* **2009**, *42*, 339–341. [CrossRef]